CHAPTER 4 RESULTS AND DISCUSSIONS

This chapter focuses on the results of heat of surface pellet simulations and experiments of alumina nanoparticles prepared by laser ablation in deionized water. The RLC simple model was created from the output laser power that obtained from long pulsed Nd:YAG laser. The effects of laser power output at surface temperature of Al pellet were simulated using MATLAB. The effects of different laser energies (1, 3, 5 and 7 J) in different voltages (300, 400 and 500 V) on physical, structure, optical and chemical properties of alumina nanoparticles were characterized. The properties of the nanoparticles were investigated by field emission scanning electron microscopy (FE-SEM), energy dispersive spectroscopy (EDS), x-ray diffraction (XRD), UV-visible spectroscopy, and x-ray photoelectron spectroscopy (XPS).

4.1 Laser energies with pulse durations at different voltages

The laser energy per pulse (J/pulse) could be obtained by adjusting pulse durations (1, 5, 10, 15 and 20 ms) of Nd:YAG laser in different voltage (250, 300, 350, 400, 450 and 500V). The plots of the laser energies of different voltages are shown in figure 4.1.

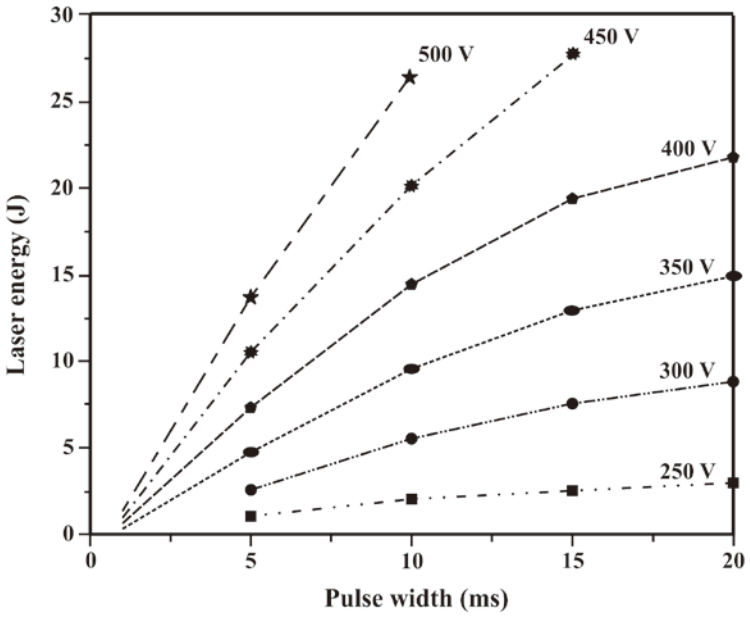

Figure 4.1 Laser energy of each voltage by adjusting pulse durations

4.2 Laser power output with pulse durations at different voltages

In figure 4.2(a)-(c), figure 4.3(a)- (c) and figure 4.4(a)- (c) show the laser power output waveforms in different setting pulse durations (1, 10 and 20 ms) of Nd:YAG laser at voltage 300 V, 400 V and 500 V respectively. The laser power output waveforms were measured by oscilloscope model Rigol DS-1100 (bandwidth 100 MHz) and the ratio of the output voltage per output power was 1 V per 1 kW. It is clearly observed that the pulse durations are nearly setting pulse duration but in different voltages are different peak powers. In the different voltages (300, 400 and 500 V), the peak output powers were about 0.7, 1.8, 3.4 kW respectively. The rise times of peak powers in all output voltages were around 2 ms and tail times were about 18 ms. The maximum adjustment of pulse duration at the voltage of 500 V was 10 ms (highest energy).

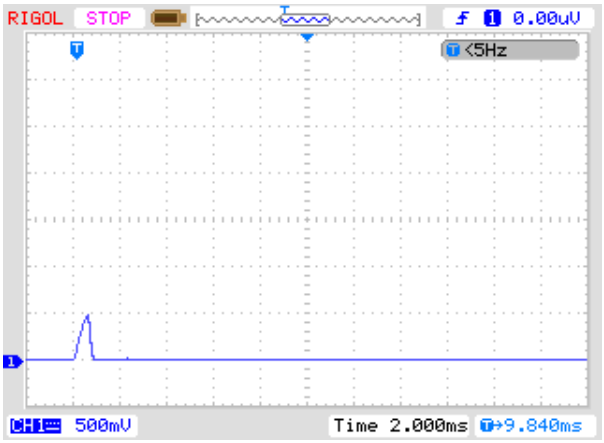

(a)

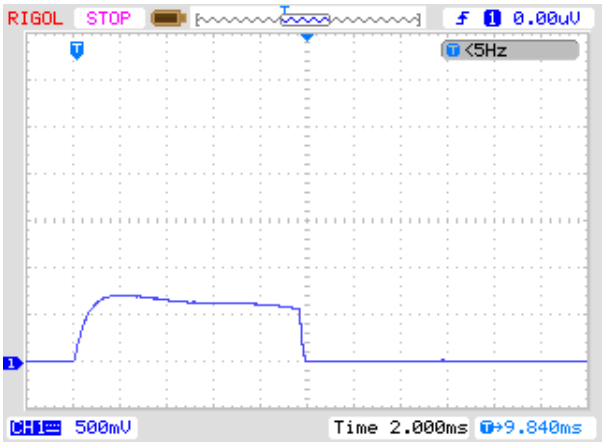

(b)

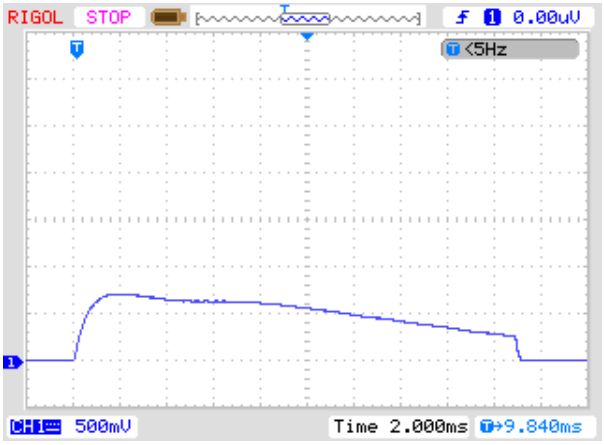

(c)

Figure 4.2 Laser power output waveform of Nd:YAG laser at 300 V a) 1 ms b) 10 ms c) 20ms (1V/1kW)

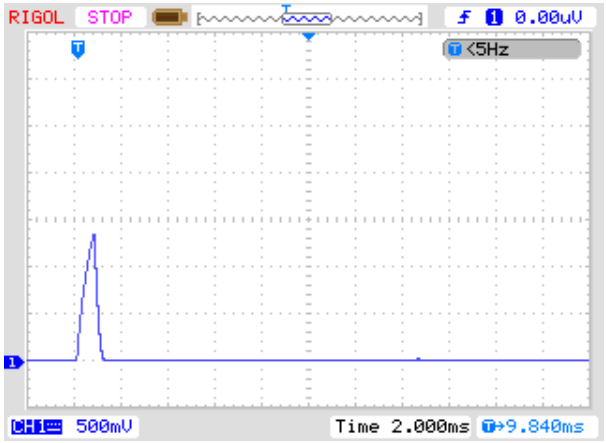

(a)

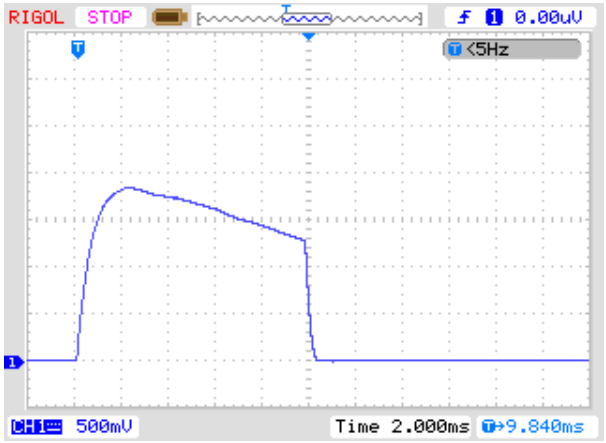

(b)

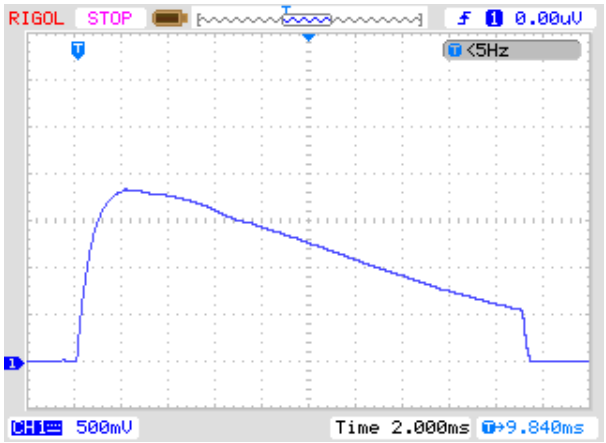

(c)

Figure 4.3 Laser power output waveform of Nd:YAG laser at 400 V a) 1 ms b) 10 ms c) 20ms (1V/1kW)

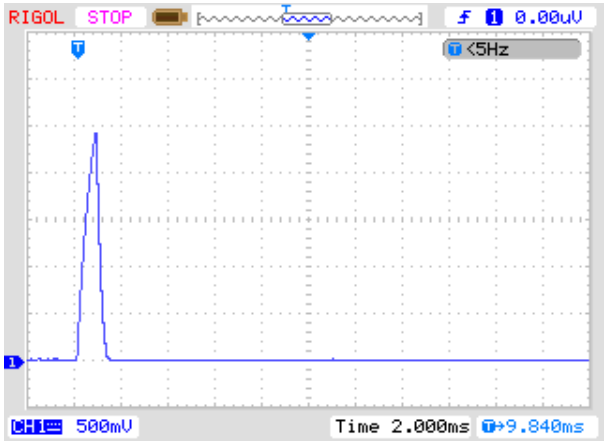

(a)

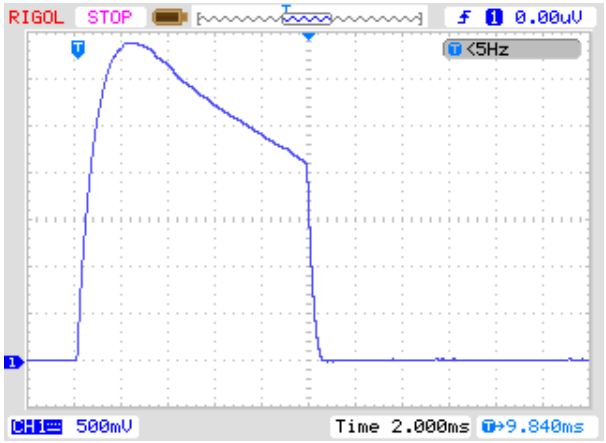

(b)

Figure 4.4 Laser power output waveform of Nd:YAG laser at 500 V a) 1 ms b) 10 ms (1V/1kW)

4.3 Curvefit of laser power output waveform

After recieved the data of laser power output waveforms from oscilloscope, the waveforms were fitted in three times using MATLAB software for finding a simple equation to represent waveforms in each different voltages (300, 400, 500V) as show in Table 4.1

Table 4.1 The curve fit of laser power output using MATLAB

equation	Voltage (V)	Parameters in equation					Number of fitting
		a	b	c	d	R^2	
$ae^{-bt} - ce^{-dt}$	300	870.5	50	963.2	1400	0.942	1st
	400	2354	65	2511	1200	0.985	
	500	4394	75	4340	1100	0.991	
$ae^{-bt} - ce^{-dt}$	300	986	65	1038	1100	0.884	2rd
	400	2367		2413		0.983	
	500	4171		3994		0.979	
$a(e^{-bt} - e^{-dt})$	300	982.4	65	-	1100	0.884	3rd
	400	2364				0.983	
	500	4187				0.979	

The approximate pulsed power output in different voltages are simplify to

$$P(t)_{300V} = 982.4(e^{-65t} - e^{-1100t})W$$
$$P(t)_{400V} = 2364(e^{-65t} - e^{-1100t})W$$
$$P(t)_{500V} = 4187(e^{-65t} - e^{-1100t})W$$

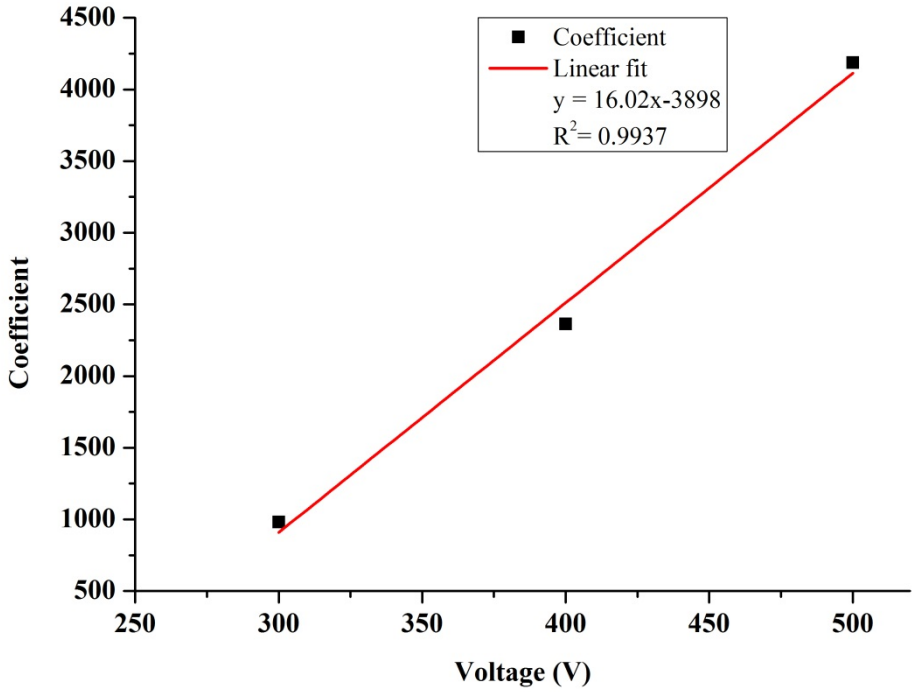

Figure 4.5 Plot of coefficient of third equation in each voltage.

Figure 4.5 show plot of coefficient of pulsed power output simplification. The relation of coefficient is linear in each voltage according with linear equation y=16.02x-3898. From P(t) in different voltages above we can find E(t) by

$$P(t) = \frac{dE(t)}{dt} \tag{4.1}$$

$$E(t) = \int P(t)dt = \int a(e^{-bt} - e^{-dt})dt$$
$$E(t)_{300V} = \int 982.4(e^{-65t} - e^{-1100t})dt = 982.4\int (e^{-65t} - e^{-1100t})dt$$
$$= 0.893e^{-1100t} - 15.114e^{-65t}J$$
$$E(t)_{400V} = \int 2364(e^{-65t} - e^{-1100t})dt = 2364\int (e^{-65t} - e^{-1100t})dt$$
$$= 2.149e^{-1100t} - 36.369e^{-65t}J$$
$$E(t)_{500V} = \int 4187(e^{-65t} - e^{-1100t})dt = 4187\int (e^{-65t} - e^{-1100t})dt$$
$$= 3.806e^{-1100t} - 64.415e^{-65t}J$$

4.4 RLC simple model

From pulsed power output P(t), we can approximate value of R, L, C from the equations in the circuit analysis R = 1.7 Ω, L = 0.9 mH, C = 24000 μF. Furthermore, we can simulate current, voltage of flashlamp and capacitor voltage from this model. The figure 4.6 show RLC circuit simulation using MATLAB/Simulink that used trigger logic to perform switch using T_{on} = 20 ms in figure 4.7.

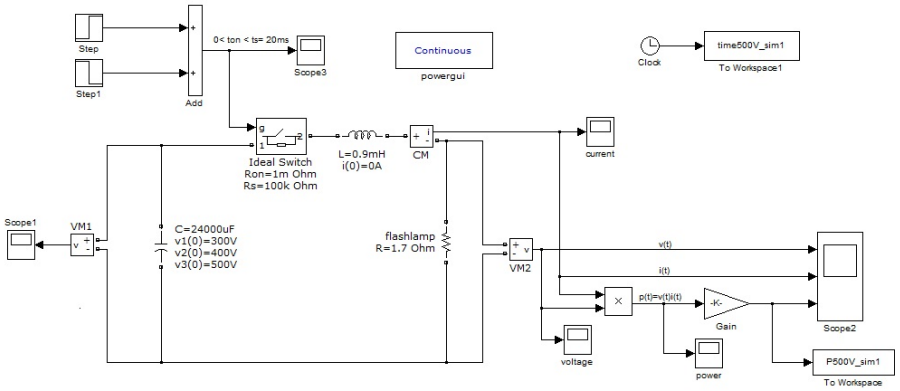

Figure 4.6 RLC circuit simulation using MATLAB/Simulink

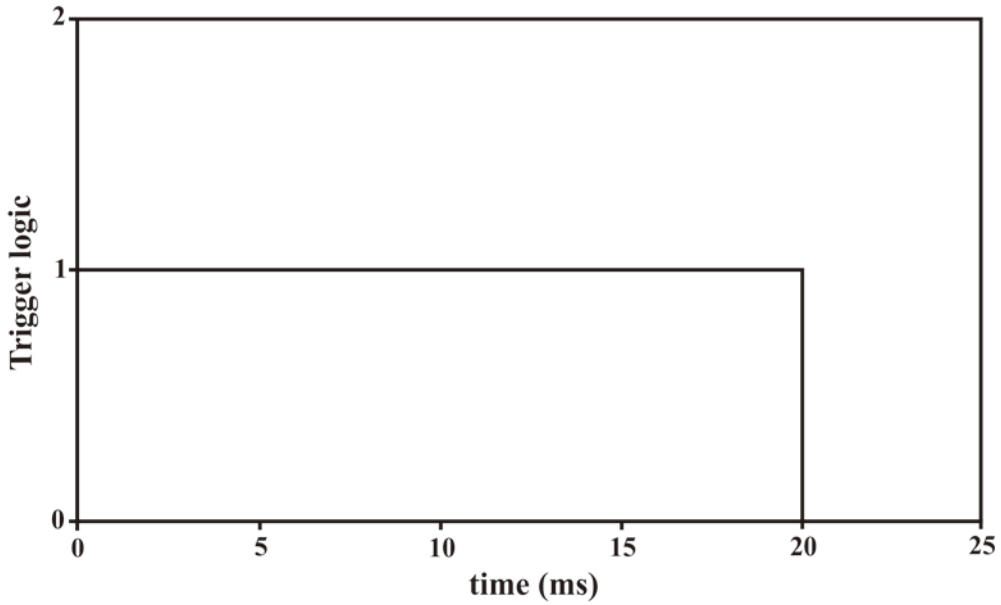

Figure 4.7 Trigger logic was performed to switch in RLC circuit.

In figure 4.8(a)-4.8(d), figure 4.9(a)-4.9(d) and figure 4.10(a)-4.10(d) show the voltage of capacitor, voltage, current and power output waveforms with pulse duration 20 ms of Nd:YAG laser at voltage 300 V, 400 V and 500 V respectively. The all output waveforms were measured using scope in MATLAB. It is clearly observed that the laser output power waveforms are closely the waveforms that obtained from the experimental results in section 4.2. The peak of capacitor voltage at t = 0 ms equal setting voltage 300, 400, 500 V. After switch was closed, the energy of capacitor transferred to inductor and resistor. The peak current is about 165, 270, 390 A respectively. The rise time to peak power in all voltage is around 2 ms and tail time is about 18 ms.

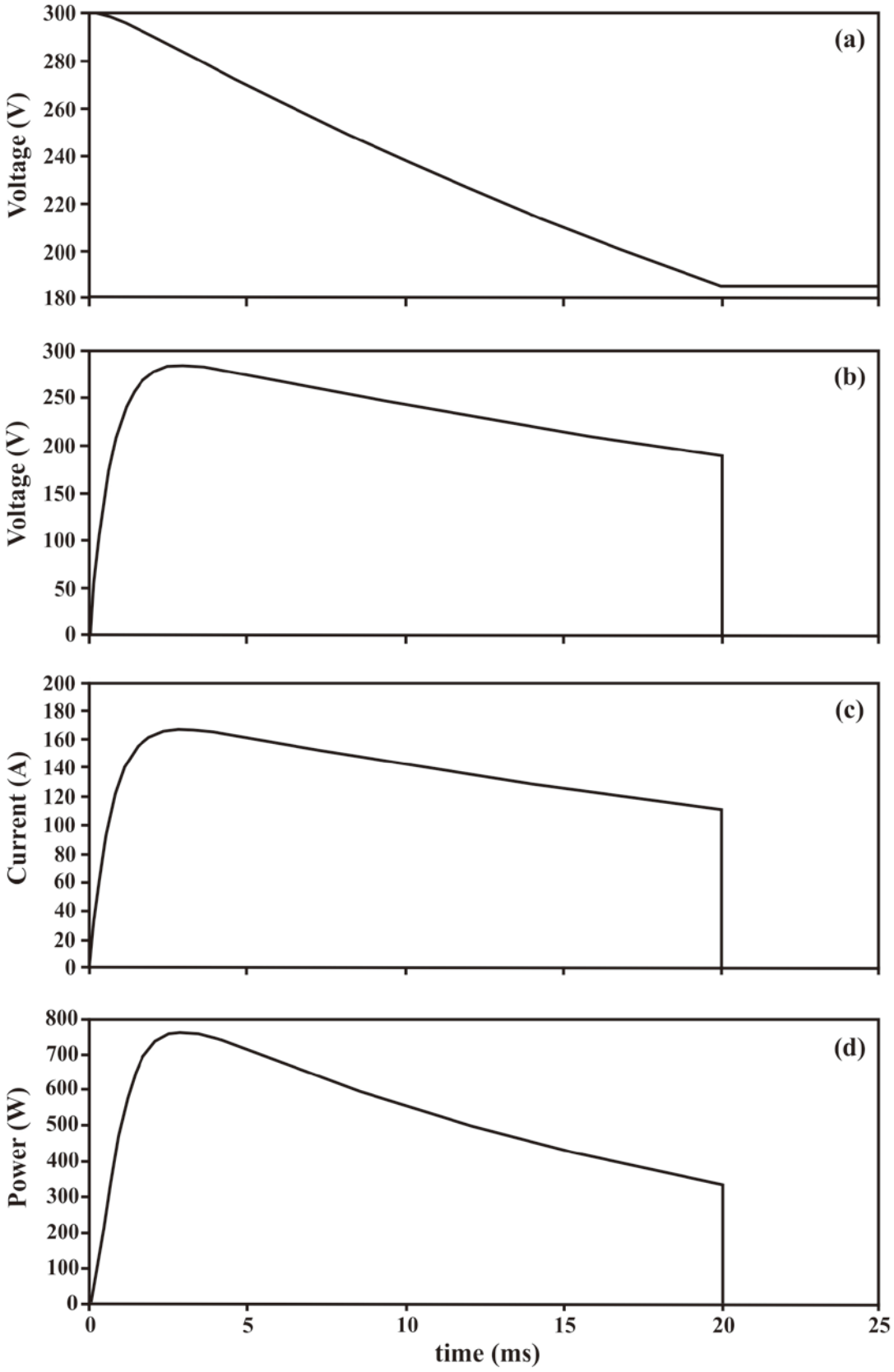

Figure 4.8 The simulation results of RLC model using MATLAB/Simulink at capacitor voltage 300 V 20 ms a) Voltage across capacitor b) Resistor voltage c) Resistor current d) Resistor power

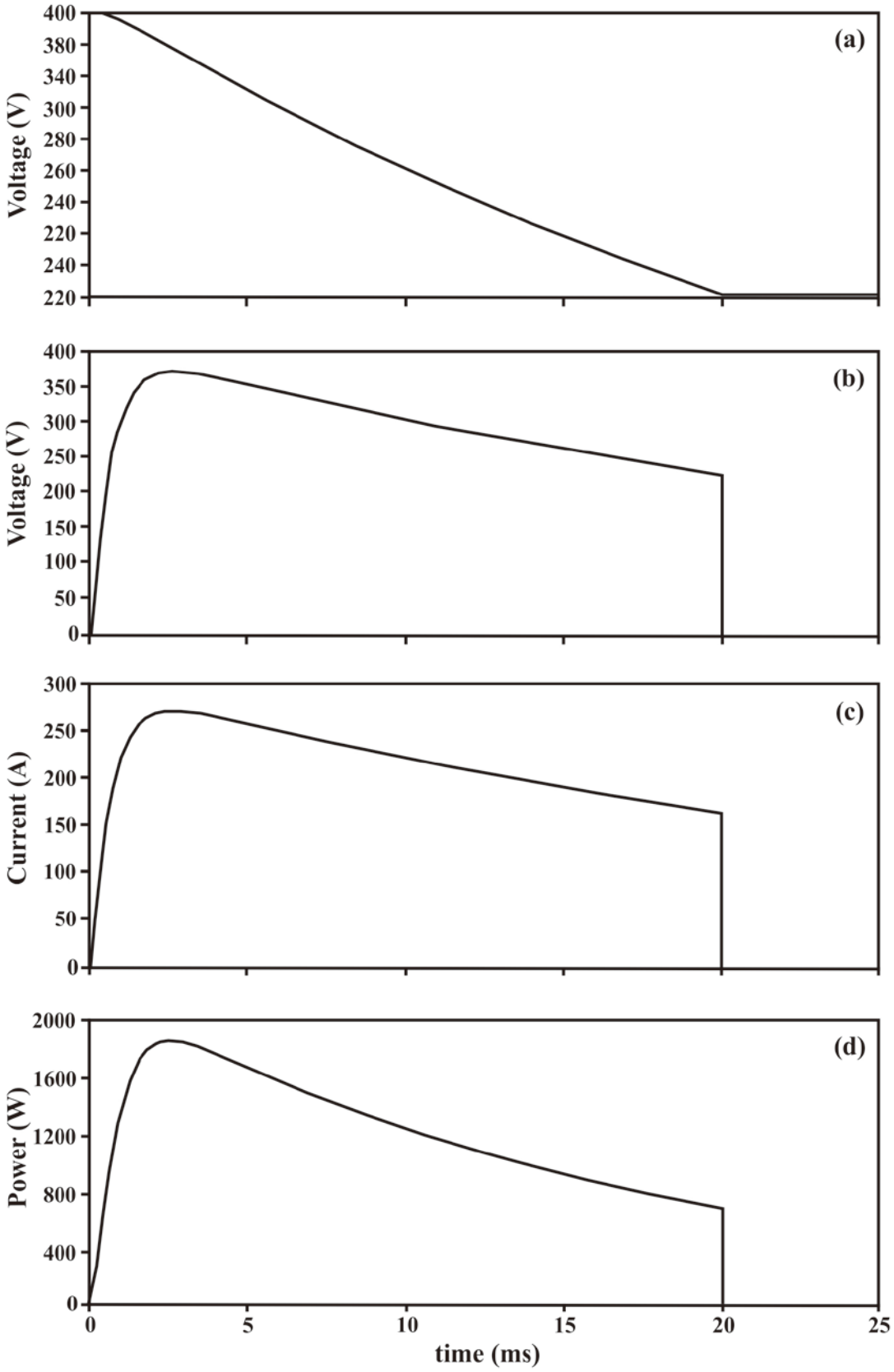

Figure 4.9 The simulation results of RLC model using MATLAB/Simulink at capacitor voltage 400 V 20 ms a) Voltage across capacitor b) Resistor voltage c) Resistor current d) Resistor power

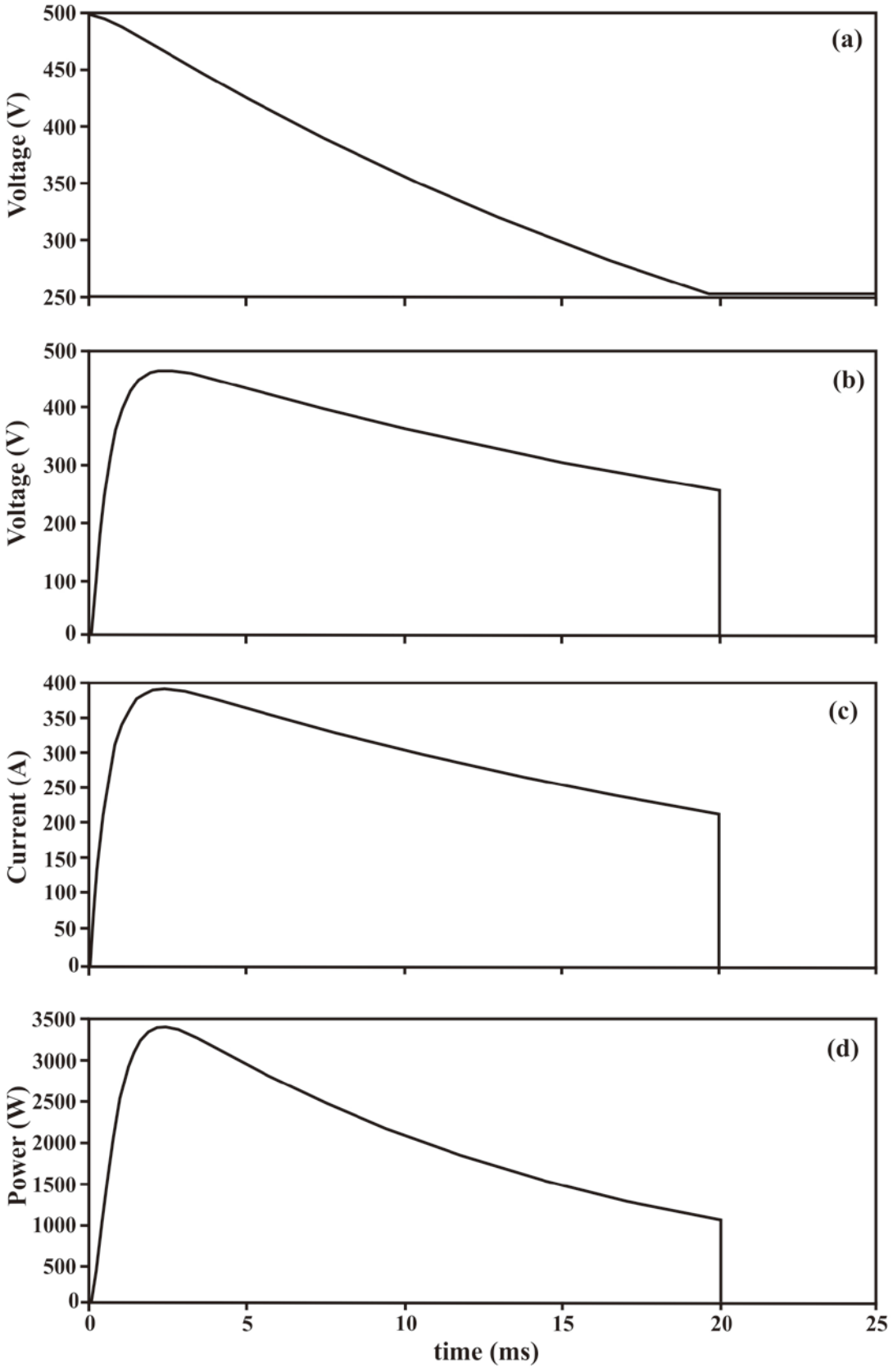

Figure 4.10 The simulation results of RLC model using MATLAB/Simulink at capacitor voltage 500 V 20 ms a) Voltage across capacitor b) Resistor voltage c) Resistor current d) Resistor power

4.5 Approximation of rectangular power from pulsed power waveform

In figure 4.11 show approximation of pulsed power output to rectangular power output in pulse duration 20 ms in different voltages 300, 400, 500 V. The rectangular power output can calculated using area of pulsed power equal area of rectangular power. In Table 4.2 show the pulse duration approximation of pulsed power in energy 1, 3, 5 J to rectangular power in different voltages 300, 400 and 500V.

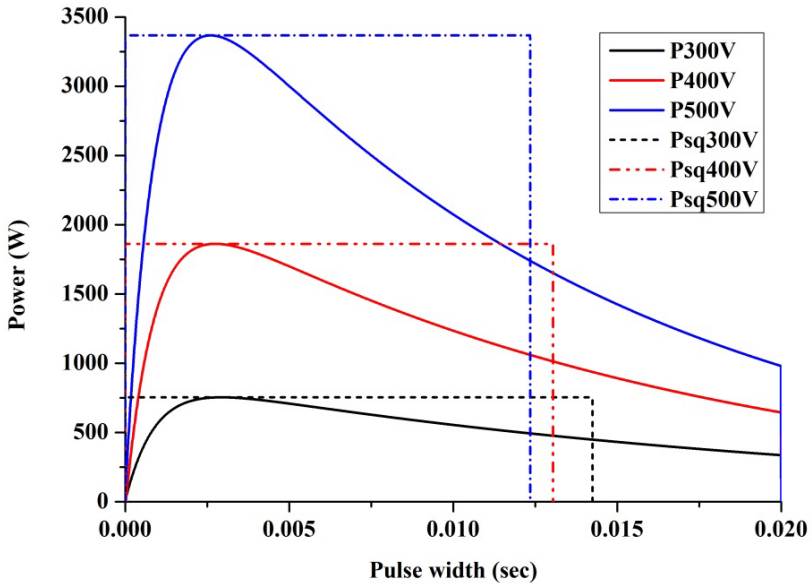

Figure 4.11 Approximation of pulsed power output to rectangular power output 20 ms in different voltages 300, 400, 500 V.

Table 4.2 Approximation of pulsed power output to rectangular power output at 1, 3 and 5 J in different voltages.

Voltage (V)	Laser energy (J/pulse)	Pulse duration in pulsed power (ms)	Pulse duration in rectangle power (ms)
300	1	2.5	1.80
	3	6.0	5.20
	5	9.7	8.10
400	1	1.5	0.95
	3	3.0	2.30
	5	4.5	3.80
500	1	0.75	0.44
	3	1.48	0.97
	5	2.11	1.50

In figure 4.12 – 4.14 are plots of approximation from pulsed power to rectangular in each energy of 1, 3, 5 J per pulse in different voltages 300, 400 and 500 V. It should to be note that the pulse durations of rectangular powers are less than the pulsed powers in all cases.

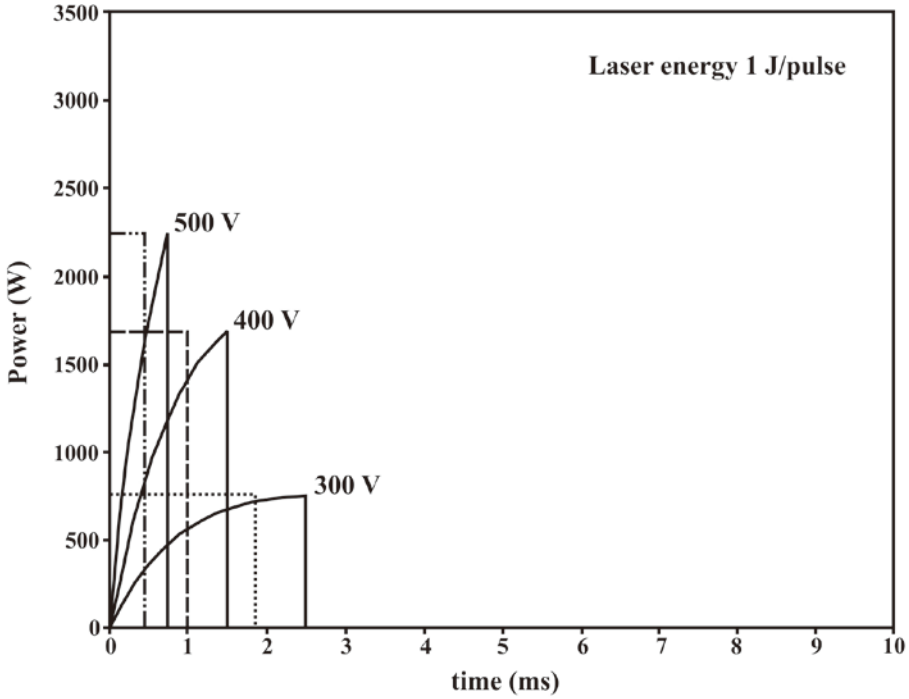

Figure 4.12 Approximation of pulsed power output to rectangle power output 1J/pulse in different voltages

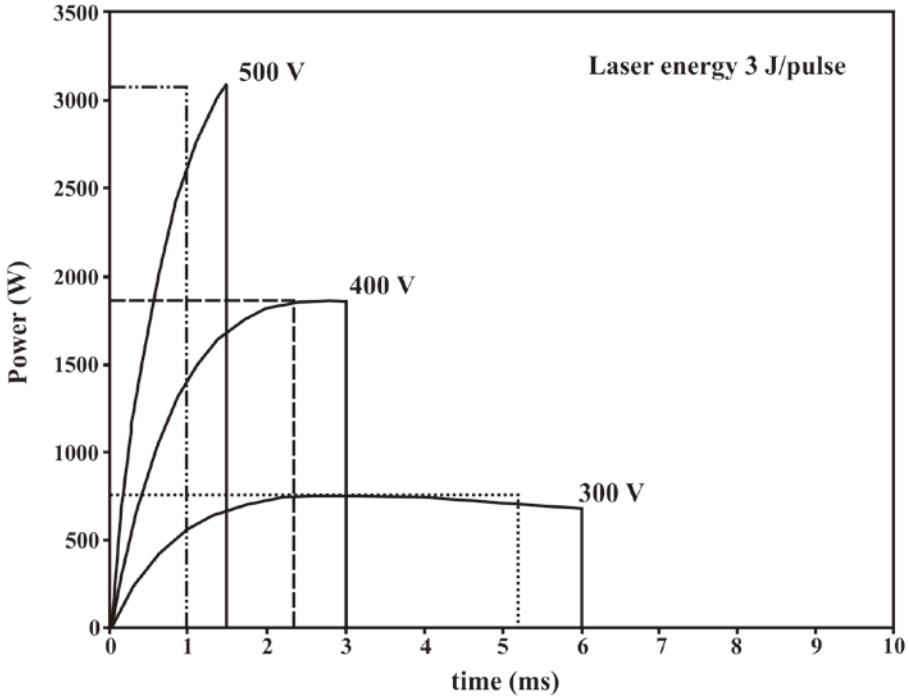

Figure 4.13 Approximation of pulsed power output to rectangular power output 3J/pulse in different voltages

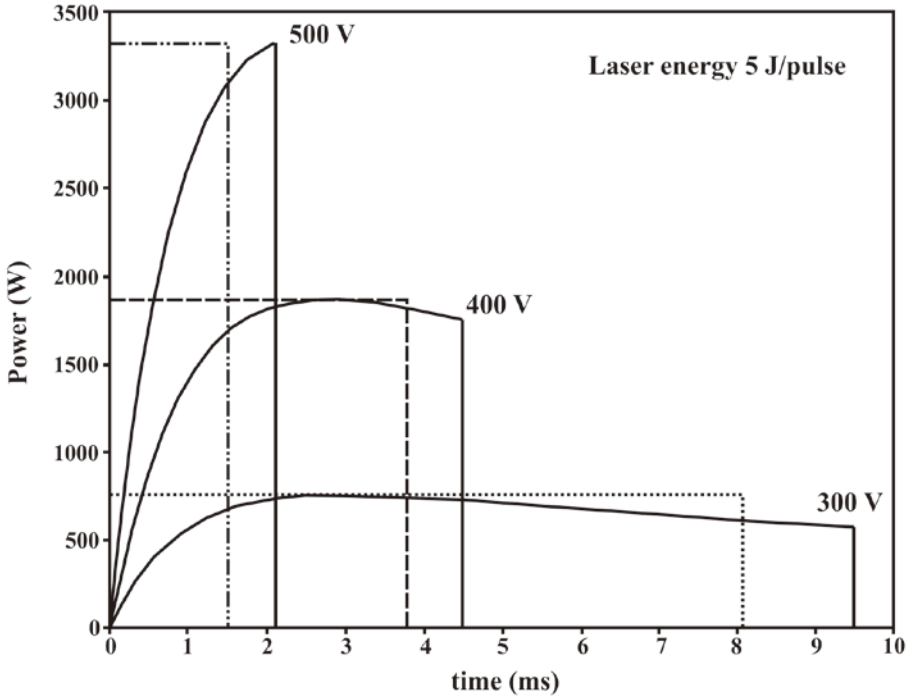

Figure 4.14 Approximation of pulsed power output to rectangular power output 5J/pulse in different voltages

4.6 Simulation of heat at surface aluminum pellet

After we got the rectangular power from pulsed power waveform in section 4.5, The heat at surface of Al pellet were simulated using heat equation from (2.16) for $t < t_{on}$ and equation (2.17) for $t > t_{on}$ with parameters k = 220 W/(m °C), ρ = 2707 kg/m^3 , A = 0.03 mm^2. In figure 4.15- 4.17 show temperature rise ($t < t_{on}$) and down ($t > t_{on}$) at 1, 3 and 5 J in different voltages 300, 400 and 500 V respectively. The peak of temperature is highest at 5 J, 500V and lowest at 1 J, 300V due to peak of power and pulse duration of 5 J, 500 V higher than 1 J 300 V

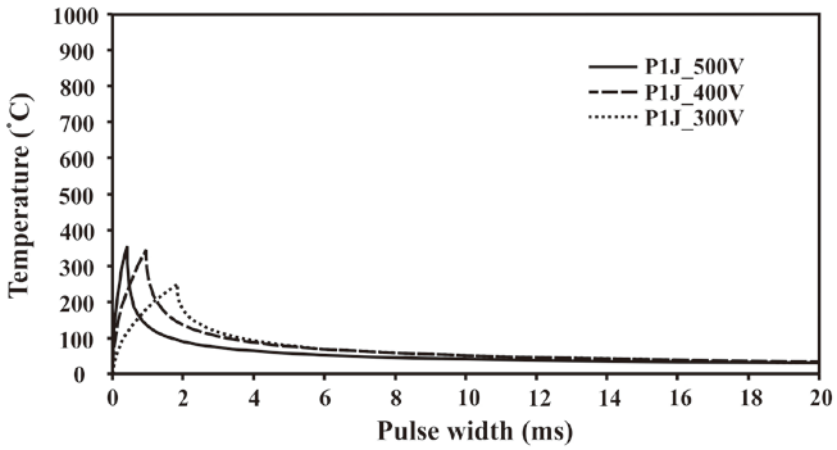

Figure 4.15 Simulation of heat at surface Al pellet from square power output 1J at 300, 400, 500 V

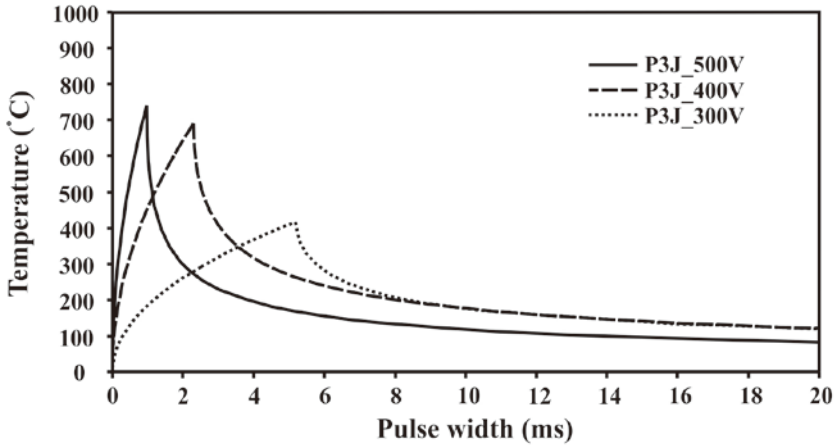

Figure 4.16 Simulation of heat at surface Al pellet from square power output 3J at 300, 400, 500 V

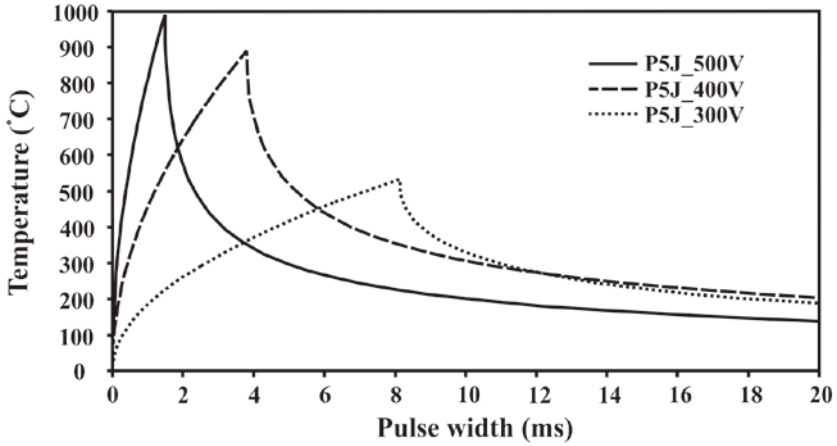

Figure 4.17 Simulation of heat at surface Al pellet from square power output 5J at 300, 400, 500 V

4.7 Experimental results of laser ablation

During the ablating process, plasma plume was formed on the surface of the aluminum pellet as shown in figure 4.18. The liquid medium has a great influence on the thermodynamical and kinetic properties of the formation of plasma plume.

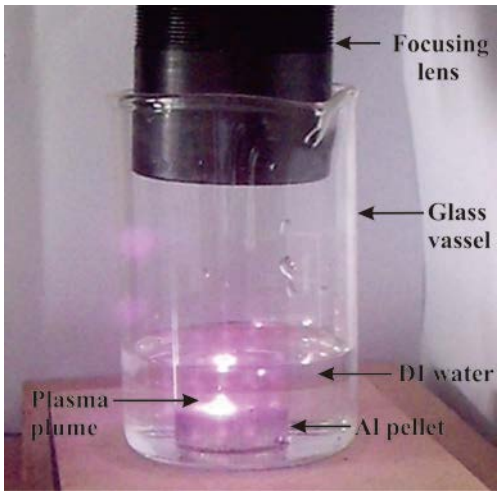

Figure 4.18 Plasma plume observed during laser ablation of aluminum target in liquid

The mechanism of alumina nanoparticles generation by the laser ablation of the aluminum pellet in the deionized water can be described in three steps [56] as shown schematically by figure 4.19. The aluminum surface was firstly heated up by the laser beam to a high temperature and high pressure (figure 4.19 (a)), then a plasma of aluminum and shock wave were formed (figure 4.19 (b)). The plasma of aluminum and deionized water were condensed. Finally alumina nanoparticles were generated (figure 4.19 (c)). During the above phenomena, the nucleation of the nanoparticles takes place and then fine nuclei of carbon stick together to grow up.

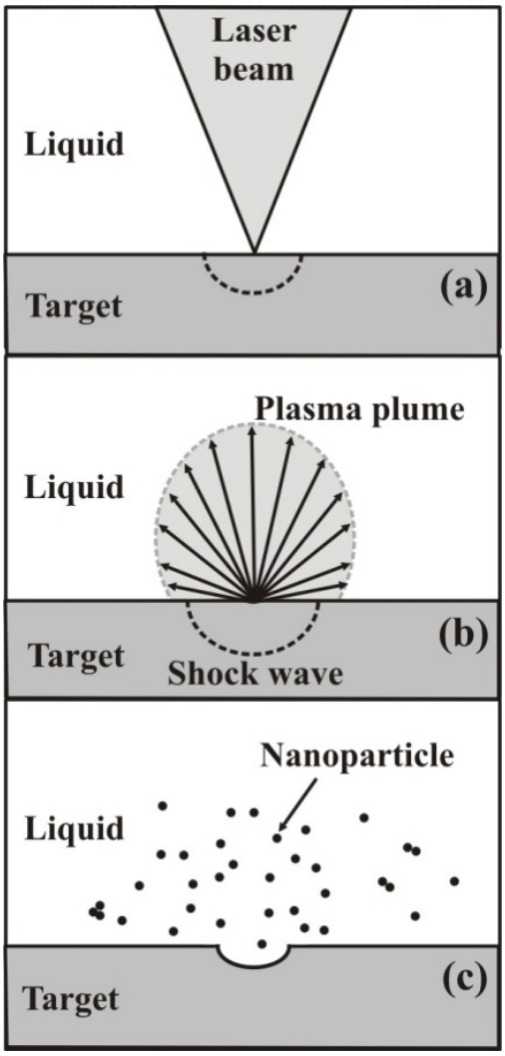

Figure 4.19 Schematically mechanism of alumina nanoparticles generation by the laser ablation in a liquid (a) target surface was heated up by the laser beam, (b) plasma plume of alumina and shock wave were formed and condensed, and (c) alumina nanoparticles were generated.

4.7.1 Effect of laser energy on the formation of alumina nanoparticles in deionized water

In this section, the different laser energies used in the synthesis of alumina nanoparticles have been studied. The laser energies employed in this study were 1, 3, 5 and 7 J/pulse. The repetition rate and number of pulse were fixed at 2 pulse per second (pps) and 5,000 pulses (about 40 min) respectively. The voltage were varied at 300, 400, 500 V and the pulse duration were adopted. The alumina nanoparticle suspensions were dropped on silicon substrate and then dried in oven at 40 °C. The morphology of alumina nanoparticles, synthesized with different laser energies and different voltages were obtained by FE-SEM. Figure 4.20 shows FE-SEM image of alumina particles in at 300 V.

It should be noted that the spot size of the laser at the target surface is 0.03 mm^2. Hence, the laser fluence (J/cm^2) can be determined and the results are given in Table 4.3

Table 4.3 Laser fluences and power densities of experiments.

Laser energy (J/pulse)	**Laser fluence (J/cm^2)**	**Power density (W/cm^2)**
1	3333	2.60×10^6
3	10000	3.33×10^6
5	16667	3.51×10^6

Figure 4.20(a) shows the FE-SEM image of the aluminum powder used as the target. It revealed that the morphology of the aluminum was a non-spherical shape with the size in the range of 1-35 µm. Figure 4.20(b) - (e) show the FE-SEM images of the alumina nanoparticles synthesized in deionized water at 300 V with different laser energies of 1, 3, 5 and 7 J, respectively. It is clearly observed that the morphology of the synthesized alumina nanoparticles is mostly spherical shape. These results are in good agreement with those previously reported in ref [33-40] However, In case of 7 J /pulse, most particles were melted by high temperature.

The particle size distribution of the alumina nanoparticles could be obtained by measuring the size of total particles of about 200 particles in the FE-SEM image using the Image J program. The particle size distribution of the alumina nanoparticles ablated from all the laser energies of 300 V are given in Table 4.4.The plots of the particle size distribution of the alumina nanoparticles are shown in Figure. 4.21. As seen in Figure. 4.20, the particle size of the alumina nanoparticles synthesized in deionized water with laser energies of 1, 3 and 5 J are ranged from 10 - 60, 10 - 70 and 10 - 110 nm, respectively. The average particle size and dominant size of the alumina nanoparticles as given in Table 4.5 showed that the smallest particle size of the alumina nanoparticles was obtained from a laser energy of 1 J and found to be 26 nm with the narrow particle size distribution in the range of 10- 60 nm. It is seen that the higher laser energy seemed to promote more collisions between the vapor atoms/ions, to coalesce within the ablated plume and eventually to form larger particles [34].

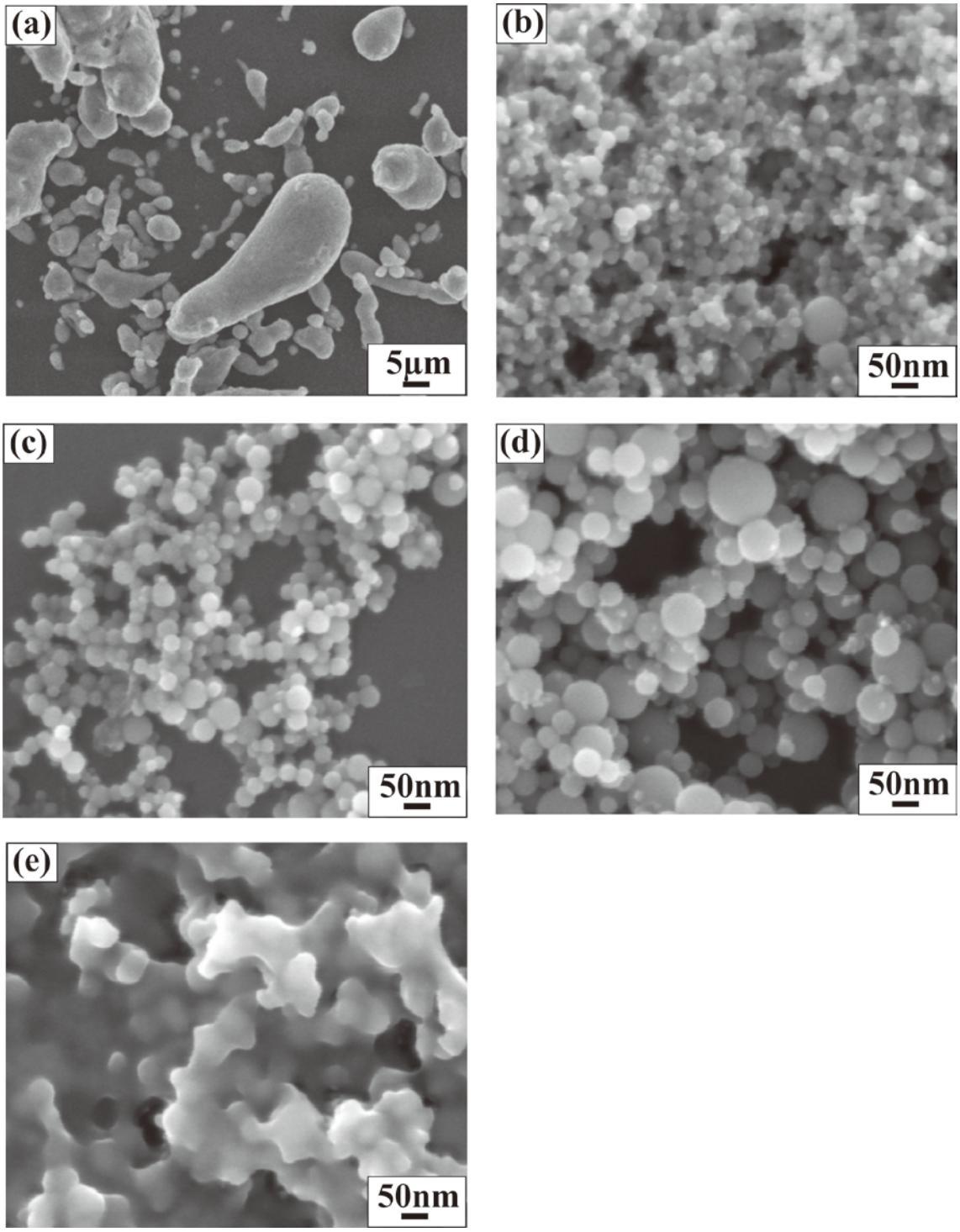

Figure 4.20 FE-SEM images of (a) aluminum powder, and alumina nanoparticles at 300 V with different laser energies of (b) 1 J, (c) 3 J (d) 5 J and (e) 7 J.

Table 4.4 The particle size distribution of the alumina nanoparticles at 300 V in all energies.

Particle size (nm)	**Number of particles**		
	300V 1 J	**300V 3 J**	**300V 5 J**
10 - 15	5	2	3
15 - 20	50	2	7
20 - 25	65	11	7
25 - 30	39	19	8
30 - 35	16	46	10
35 - 40	12	57	19
40 - 45	4	24	20
45 - 50	4	22	22
50 - 55	3	8	25
55 - 60	2	5	19
60 - 65	-	3	13
65 - 70	-	1	11
70 - 75	-	-	9
75 - 80	-	-	7
80 - 85	-	-	5
85 - 90	-	-	4
90 - 95	-	-	4
95 - 100	-	-	3
100 - 105	-	-	3
105 - 110	-	-	1
Total	200	200	200

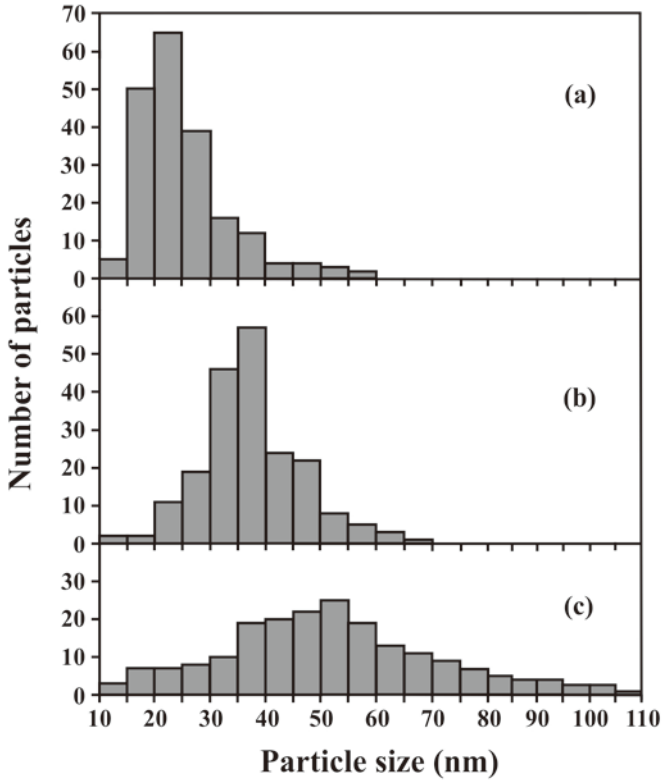

Figure 4.21 Plot of particle size distribution of alumina nanoparticles at 300 V with different laser energies: (a) 1 J/pulse, (b) 3 J/pulse and (c) 5 J/pulse

Table 4.5 Average and dominant size of nanoparticles at 300 V in different energies.

Energy at 300V (J)	Average size (nm)	Dominant size (nm)
1	26	23
3	38	38
5	53	53
7	-	-

Figure 4.21(a)-(c) show the FE-SEM images of the alumina nanoparticles synthesized in deionized water at 400 V with different laser energies of 1, 3 and 5 J, respectively. The synthesized alumina nanoparticles were mostly spherical shape but in case of 5 J, almost particles were melted by high temperature.

The particle size distribution of the alumina nanoparticles ablated from all the laser energies of 400 and 500 V are given in Table 4.5. The plots of the particle size distribution of the alumina nanoparticles are shown in Figure. 4.24. As seen in Figure. 4.22, the particle size of the alumina nanoparticles synthesized in deionized water with laser energies at 400 V of 1 and 3 J are ranged from 10 – 90 and 10 - 150, respectively. The particle size of the alumina nanoparticles synthesized in deionized water with laser energies at 500 V of 1 J are ranged from 10 – 150 nm. The average particle size and dominant size of the alumina nanoparticles at 400, 500 V as given in Table 4.7 and Table 4.8.

Table 4.6 The particle size distribution of the alumina nanoparticles at 400, 500 V in all energies.

Particle size (nm)	**Number of particles**		
	400 V 1 J	**400 V 3 J**	**500 V 1 J**
10 - 15	2	3	4
15 - 20	5	6	7
20 - 25	11	11	13
25 – 30	28	20	17
30 – 35	47	21	21
35 – 40	45	25	23
40 – 45	20	20	26
45 – 50	19	17	18
50 – 55	9	11	13
55 – 60	4	10	9
60 – 65	3	9	7
65 – 70	2	8	7
70 – 75	2	7	6
75 – 80	1	6	5
80 – 85	1	5	4
85 – 90	1	4	3
90 – 95	-	4	3
95 – 100	-	4	2
100 - 105	-	3	2
105 – 110	-	3	2
110 – 115	-	2	2
115 - 120	-	2	1
120 - 125	-	1	1
125 - 130	-	1	1
130 - 135	-	1	1
135 - 140	-	1	1
140 - 145	-	1	1
145 - 150	-	1	1
Total	200	200	200

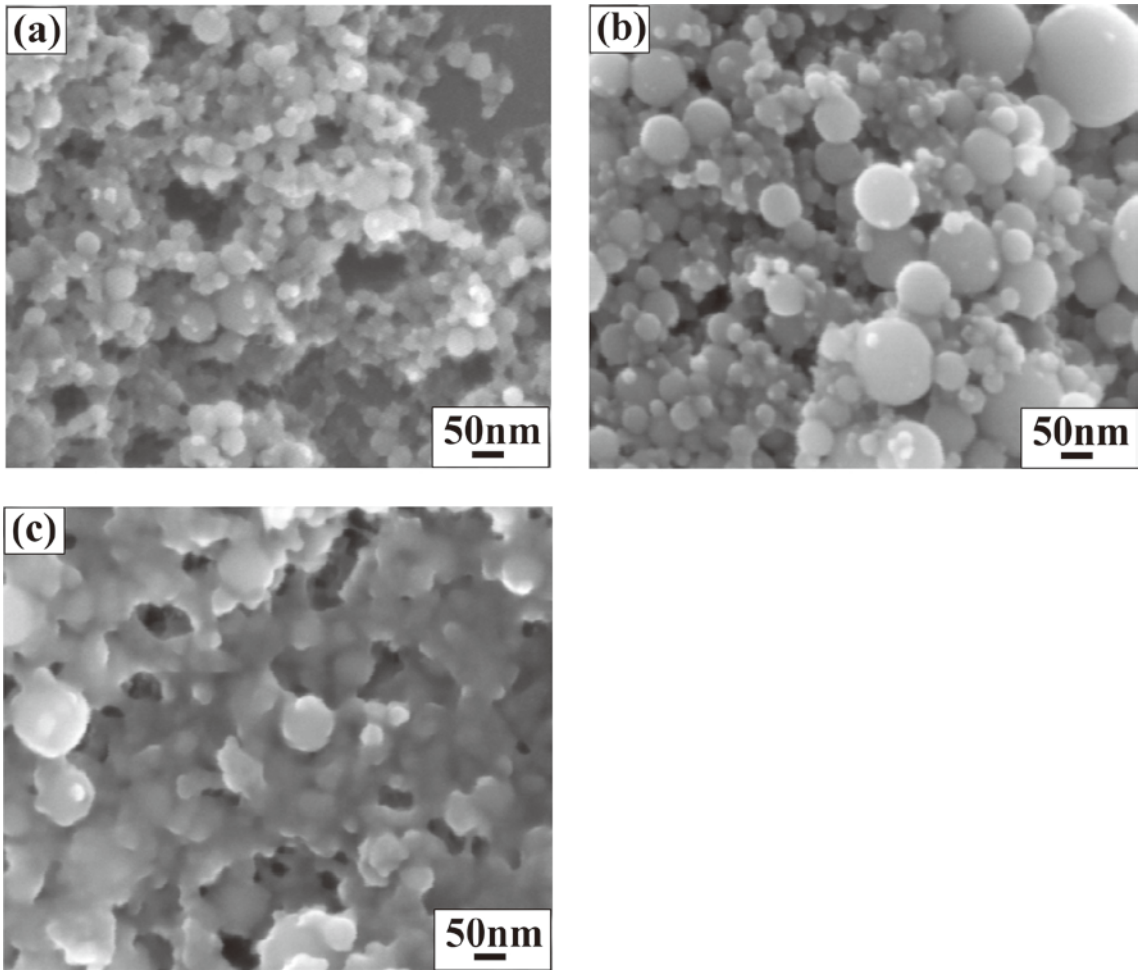

Figure 4.22 FE-SEM images of alumina nanoparticles at 400 V with different laser energies of (a) 1 J, (c) 3 J and (d) 5 J.

Table 4.7 Average and dominant size of nanoparticles at 400 V in different energies.

Energy at 400V (J)	Average size (nm)	Dominant size (nm)
1	38	33
3	53	38
5	-	-

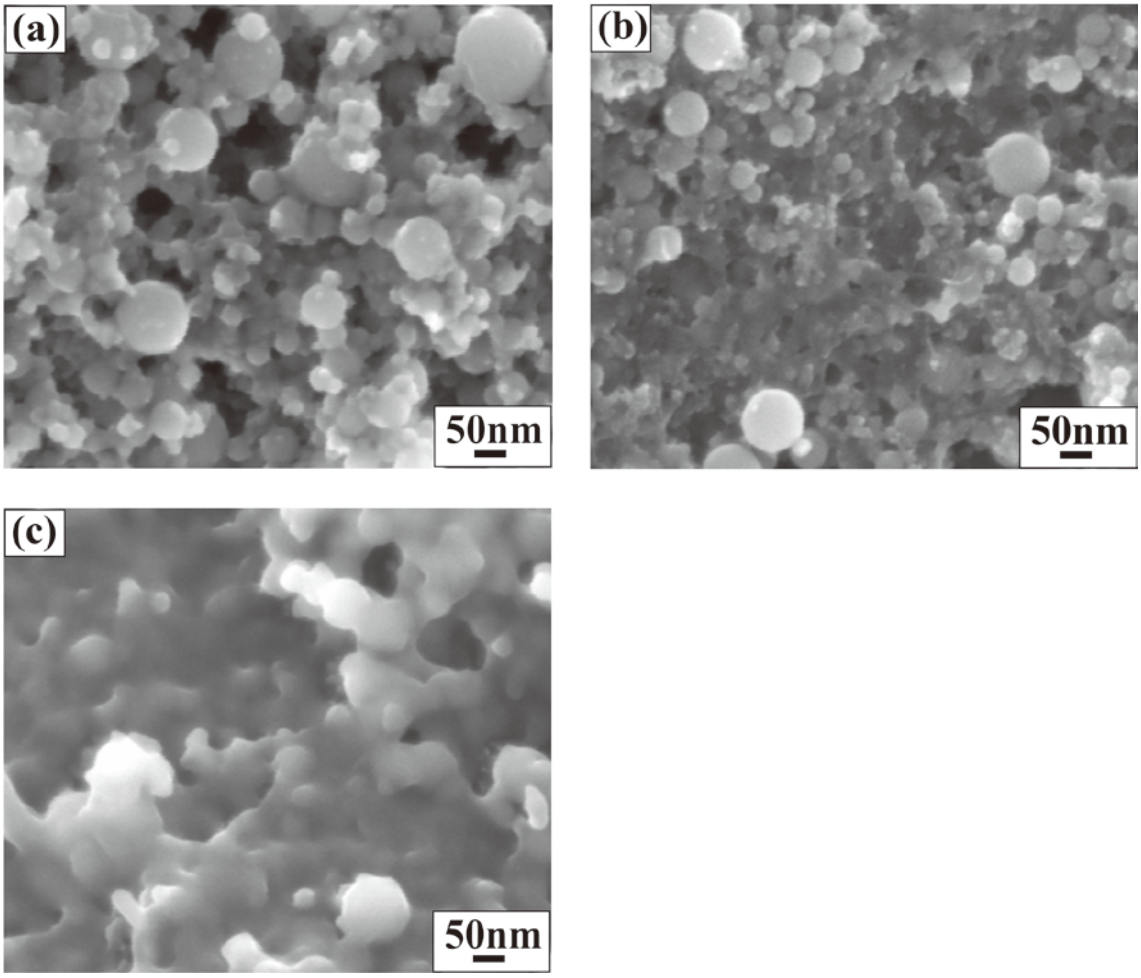

Figure 4.23 FE-SEM images of alumina nanoparticles at 500 V with different laser energies of (a) 1 J, (c) 3 J and (d) 5 J.

Table 4.8 Average and dominant size of nanoparticles at 500 V in different energies.

Energy at 500V (J)	Average size (nm)	Dominant size (nm)
1	48	43
3	-	-
5	-	-

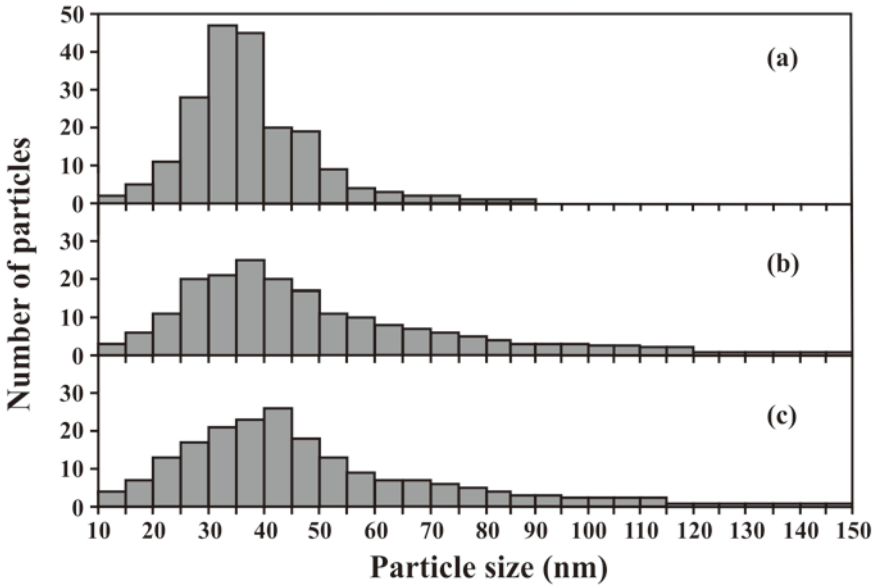

Figure 4.24 Plot of particle size distribution of alumina nanoparticles at 400 V with different laser energies: (a) 1 J/pulse, (b) 3 J/pulse and 500 V: (c) 1 J/pulse

4.7.2 Effect of repetition rate on the formation of alumina nanoparticles in deionized water

In this section, the different repetition rates used in the synthesis of alumina nanoparticles have been studied. The repetition rates employed in this study were 10 and 18 Hz. The laser energy, voltage and ablation time were fixed at 1 J/pulse, 300 V and 40 min respectively.

Figure 4.25(a)-(b) show the FE-SEM images of the alumina nanoparticles synthesized in deionized water at 300 V with repetition rates of 10 and 18 Hz, respectively. The synthesized alumina nanoparticles were mostly spherical shape but the alumina nanoparticle sizes were less than previous section (4.7.1) that repetition rate is 2 Hz.
These results according to reference [41], increase of number of pulse or ablation time results in the increase of nanoparticle concentration, relatively high number of nanoparticles screens the target, which leads to less energy absorption by it and reduction of ablation rate. Besides, primarily synthesized nanoparticles, which block the laser path, absorb a fraction of its high energy and become finer as a result of occurrence of fragmentation mechanism.

The particle size distribution of the alumina nanoparticles ablated from all the repetition rates of 10 and 18 Hz are given in Table 4.9. The plots of the particle size distribution of the alumina nanoparticles are shown in Figure. 4.26. As seen in Figure. 4.25, the particle size of the alumina nanoparticles synthesized in deionized water with laser energies at 300 V, 1 J of 10 and 18 Hz are ranged from 10 – 45 and 10 – 35 nm, respectively. The average particle size and dominant size of the alumina nanoparticles at 300 V, 1 J with 10 and 15 Hz as given in Table 4.10

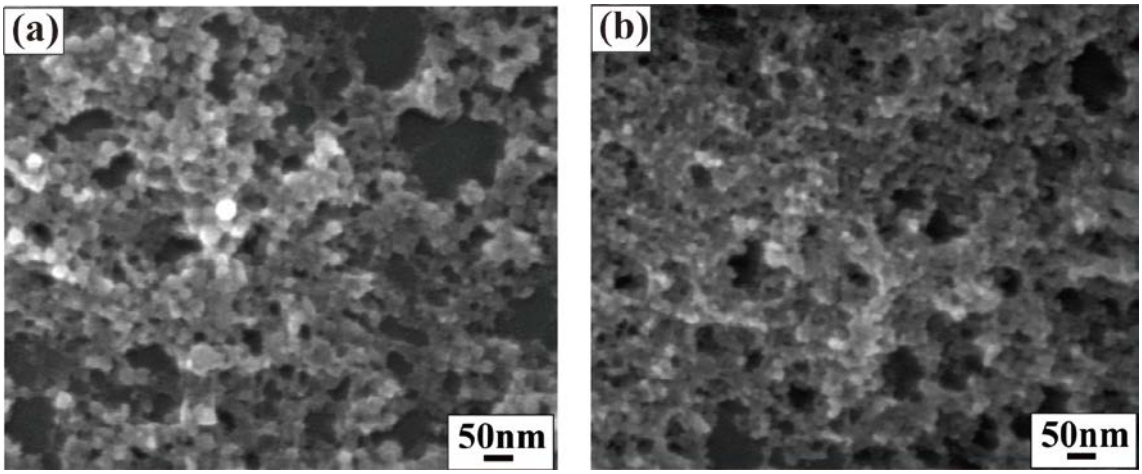

Figure 4.25 FE-SEM images of alumina nanoparticles synthesized at 300 V, 1 J with different repetition rates: (a) 10 Hz and (b) 18 Hz

Table 4.9 The particle size distribution of the alumina nanoparticles at 300 V, 1 J in different repetition rates.

Particle size (nm)	**Number of particles**	
	10 Hz	**18 Hz**
10 - 15	50	92
15 - 20	71	59
20 - 25	45	35
25 – 30	18	10
30 – 35	8	4
35 – 40	5	-
40 – 45	3	-
45 – 50	-	-
Total	200	200

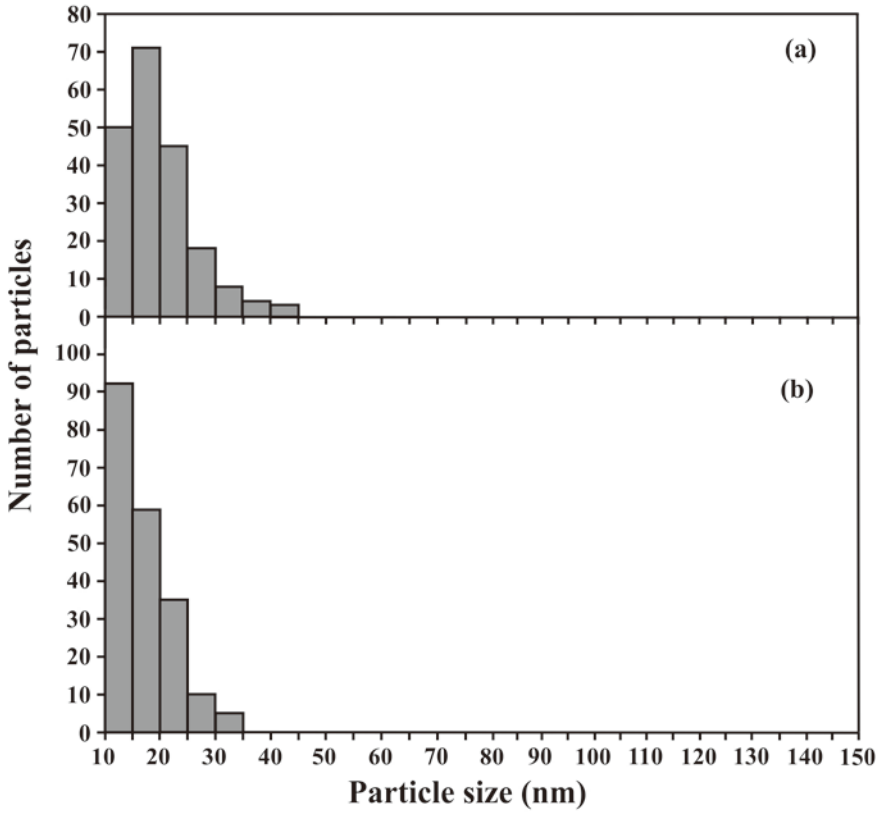

Figure 4.26 Plot of particle size distribution of alumina nanoparticles at 300 V, 1 J with different repetition rates (a) 10 Hz (b) 18 Hz

Table 4.10 Average and dominant size of nanoparticles at 300 V in different repetition rates.

Repetition rate at 300 V (1 J)	Average size (nm)	Dominant size (nm)
10	19	17
18	15	13

4.7.3 Chemical composition analysis using EDS

Chemical compositions of the alumina nanoparticles were investigated using EDS in FE-SEM in different scanning areas mode (figure 4.27). Two elements of aluminium and oxygen were detected, exclusive of the silicon substrate signals as shown in Table 4.11. The average ratios of aluminium to oxygen were close to 2:3, supporting the formation of stoichiometric Al_2O_3.

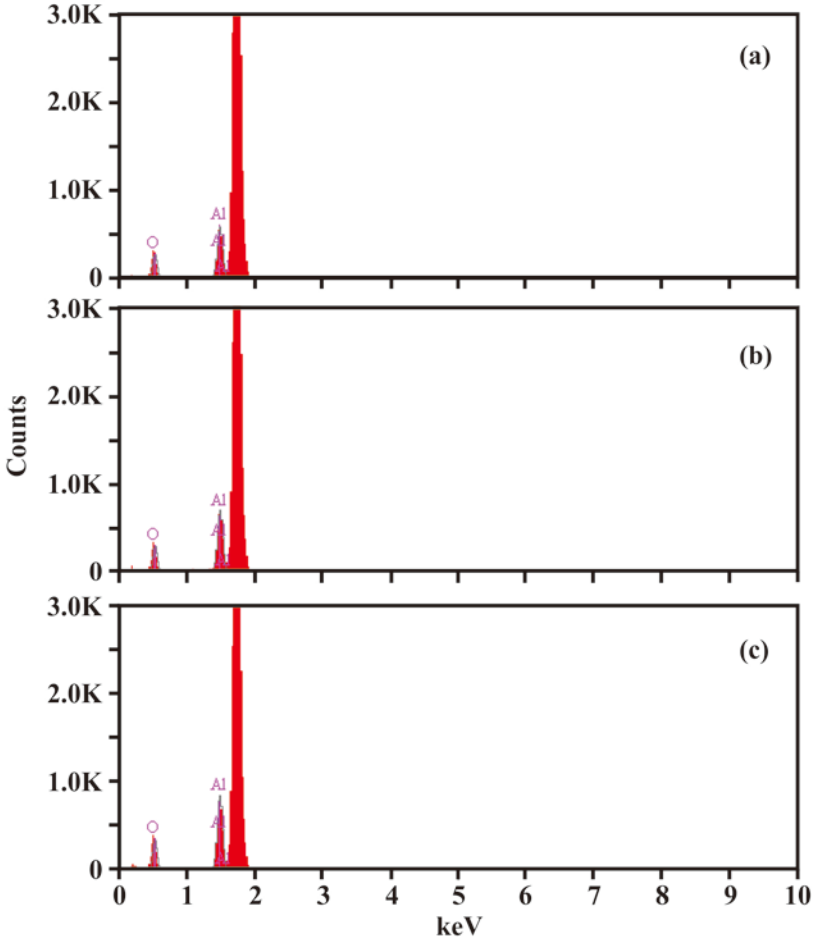

Figure 4.27 EDS results of laser energies 1, 3, 5 J at 300 V

Table 4.11 EDS results of chemical compositions at 300 V

Laser energy (J/Pulse)	Element	Atomic percentage %
1	Al	38.2
	O	61.8
3	Al	41.5
	O	58.5
5	Al	37.8
	O	63.2

4.7.4 Effect of different laser energies at 300 V on optical properties of alumina nanoparticles

Figure 4.28 shows the opacity of deionized water after the laser ablation of Al with different laser energies. It is clearly observed that the opacity of deionized water increases with increasing laser energy. It can be concluded that the opacity of deionized water is proportional to the number of alumina nanoparticles suspended in deionized water. Hence, the alumina nanoparticles obtained from a laser energy of 5 J are higher than those obtained from 3 and 1 J. Figure 4.29 shows the absorption spectra of deionized water with suspended Al2O3 nanoparticles obtained from laser energies of 1,

3, and 5 J. A strong absorption peak at 210nm is clearly observed which confirms the presence of Al2O3 nanoparticles in deionized water [57, 58] and not those of aluminum [27, 38, 59]. As seen in Figure 6, the difference of absorbance is due to the different Al2O3 nanoparticle concentrations suspended in deionized water.

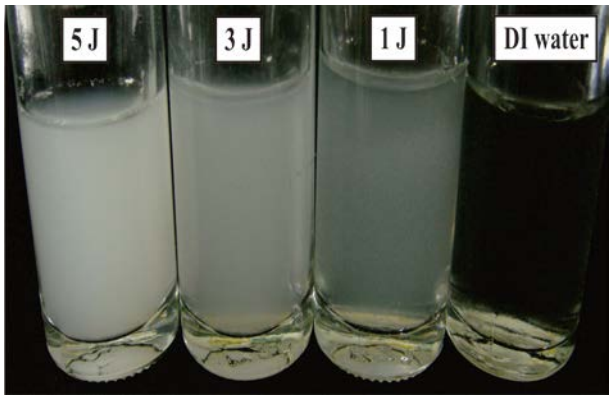

Figure 4.28 Alumina nanoparticles dispersed in deionized water at 300V after 5000 pulses of laser ablation

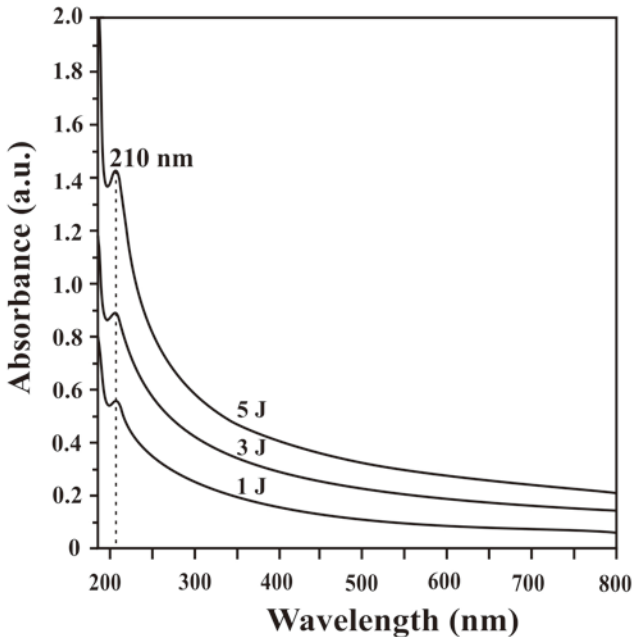

Figure 4.29 Absorption spectra in deionized water with suspended alumina nanoparticles prepared from different laser energies of 1, 3 and 5 J.

To confirm the dependence of the absorbance on the alumina nanoparticle concentration, all the samples of deionized water with suspended alumina nanoparticles were diluted with deionized water to obtain different water concentrations of C/2, C/4, C/8, and C/16, where C is the initial concentration. All the diluted deionized water samples were used for absorption measurements.

Figure 4.30-4.32 shows the typical absorption spectra of the deionized water with different alumina nanoparticle concentrations obtained from different laser energies of 1, 3 and 5 J, respectively. It is seen that the absorbance decreases with decreasing concentration. The plot between alumina nanoparticle concentration and absorbance in all energies were shown in Figure 4.33. Figure 4.33 shows that the absorbance depends linearly on the Al2O3 nanoparticle concentration. Similar results were also obtained for all laser energies.

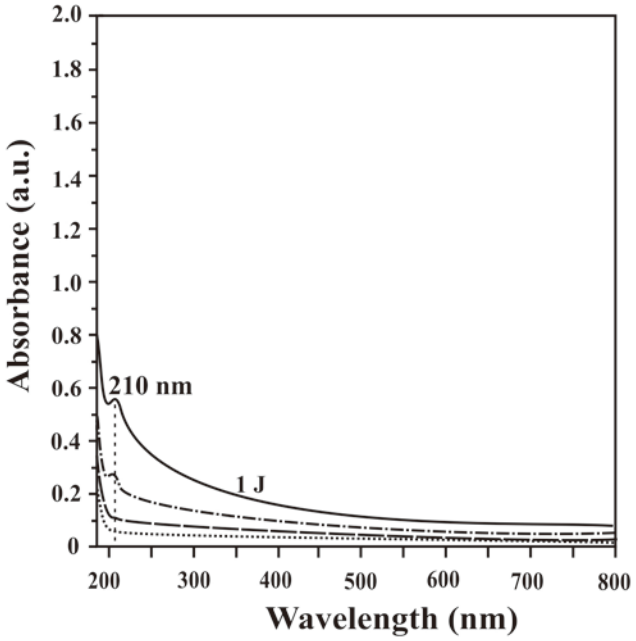

Figure 4.30 Absorption spectra in deionized water with suspended alumina nanoparticles prepared from laser energy of 1J.

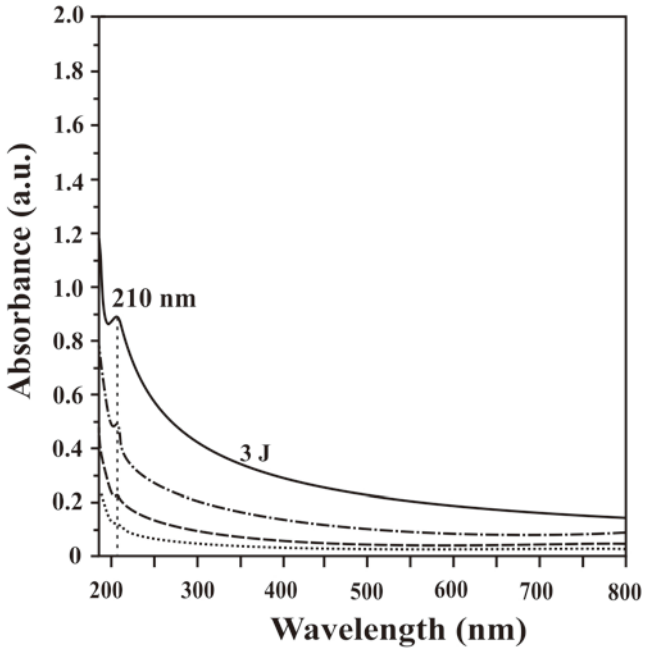

Figure 4.31 Absorption spectra in deionized water with suspended alumina nanoparticles prepared from laser energy of 3 J.

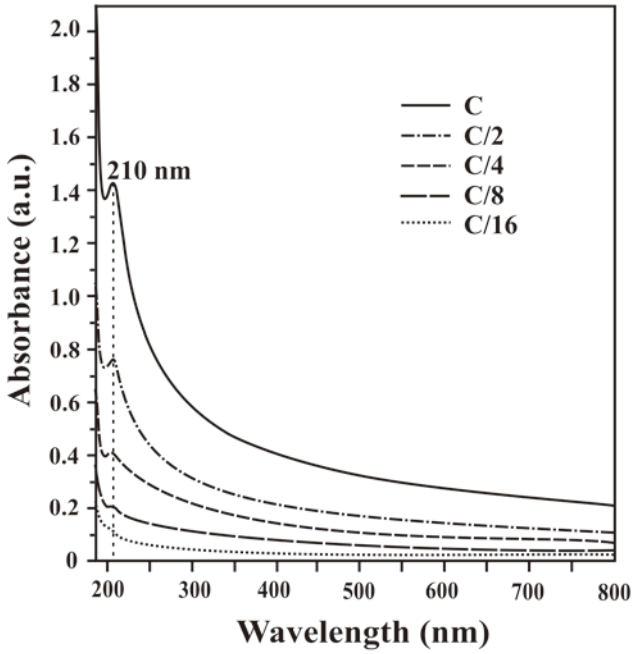

Figure 4.32 Absorption spectra in deionized water with suspended alumina nanoparticles prepared from laser energy of 5 J.

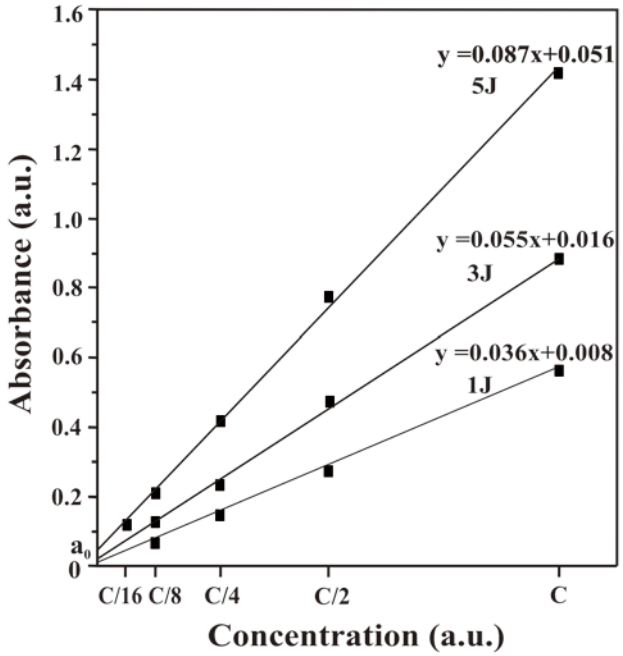

Figure 4.33 Linear relationship between the absorbance and the concentration at wavelength 210 nm.

The relation between absorbance (A) and liquid concentration (C) is given by

$$A = \varepsilon C \ell \quad (4.1)$$

A plot of absorbance at a given wavelength vs. concentration gives a straight line with a slope of $\varepsilon \ell$ (Recall that the equation for a straight line is y = mx + b.). In this case, y is the absorbance and x is the concentration. The y-intercept (b) is zero (in theory but not necessary for experimental data).

For alumina nanoparticles at 300 V, 5 J, A cell has path length (ℓ) of 1 cm. The absorbance of the solution at the wavelength of 210 nm is 1.425. A value for molar absorptivity (ε) is 0.087 L mol^{-1} cm^{-1} then the concentration is given by;

$$C = \frac{A}{\varepsilon \ell} = \frac{a - a_0}{\varepsilon \ell}$$

$$= \frac{1.425 - 0.051}{0.087 \times 1}$$

$$= 15.793 \text{ mol } L^{-1}$$

For Al_2O_3 nanoparticles at 300 V, 3 J, A cell has path length (ℓ) of 1 cm. The absorbance of the solution at the wavelength of 210 nm is 0.872. A value for molar absorptivity (ε) is 0.055 L mol^{-1} cm^{-1} then the concentration is given by;

$$C = \frac{A}{\varepsilon \ell} = \frac{a - a_0}{\varepsilon \ell}$$

$$= \frac{0.872 - 0.016}{0.055 \times 1}$$

$$= 15.564 \text{ mol } L^{-1}$$

For Al_2O_3 nanoparticles at 300 V, 1 J, A cell has path length (ℓ) of 1 cm. The absorbance of the solution at the wavelength of 210 nm is 0.562. A value for molar absorptivity (ε) is 0.036 L mol^{-1} cm^{-1} then the concentration is given by;

$$C = \frac{A}{\varepsilon \ell} = \frac{a - a_0}{\varepsilon \ell}$$

$$= \frac{0.562 - 0.008}{0.036 \times 1}$$

$$= 15.389 \text{ mol } L^{-1}$$

4.7.5 Structural characterization

The structure of ablated particles was investigated by XRD measurement. To identify the structural difference between ablated particles and Al, the XRD measurement for Al target was also carried out. Figure 4.34 shows the XRD patterns of Al target and particles synthesized from laser energies of 1, 3 and 5 J. The observed peaks in Fig.2 could be indexed based on pure Al and γ-Al_2O_3 phase in Joint Committee on Powder Diffraction Standard - International Center for Diffraction Data (JCPDS-ICDD) card nos. 85-1327 and 29-0063, respectively. It is seen from the XRD spectra that all particles obtained from laser ablation with different laser energies are γ-Al_2O_3. This confirms that Al transformed into γ-Al_2O_3 after the ablation in deionized water. Moreover, it is clearly observed that the intensity of XRD peaks increased with increasing laser energy. This might lead to the conclusion that the particle concentration, suspended in deionized water, obtained from a laser energy of 5 J is higher than those of 1 and 3 J.

It should be pointed out that the phase transitions in aluminum oxide occur in the following order [46]:

$$\gamma\text{-}Al_2O_3 \rightarrow \delta\text{-}Al_2O_3 \rightarrow \theta\text{-}Al_2O_3 \rightarrow \alpha\text{-}Al_2O_3$$

Since γ-Al_2O_3 occurs at the lowest temperature compared with those of another phases, therefore the most likely phase of Al_2O_3 to be formed after laser ablation of Al target in deionized water is γ-Al_2O_3.

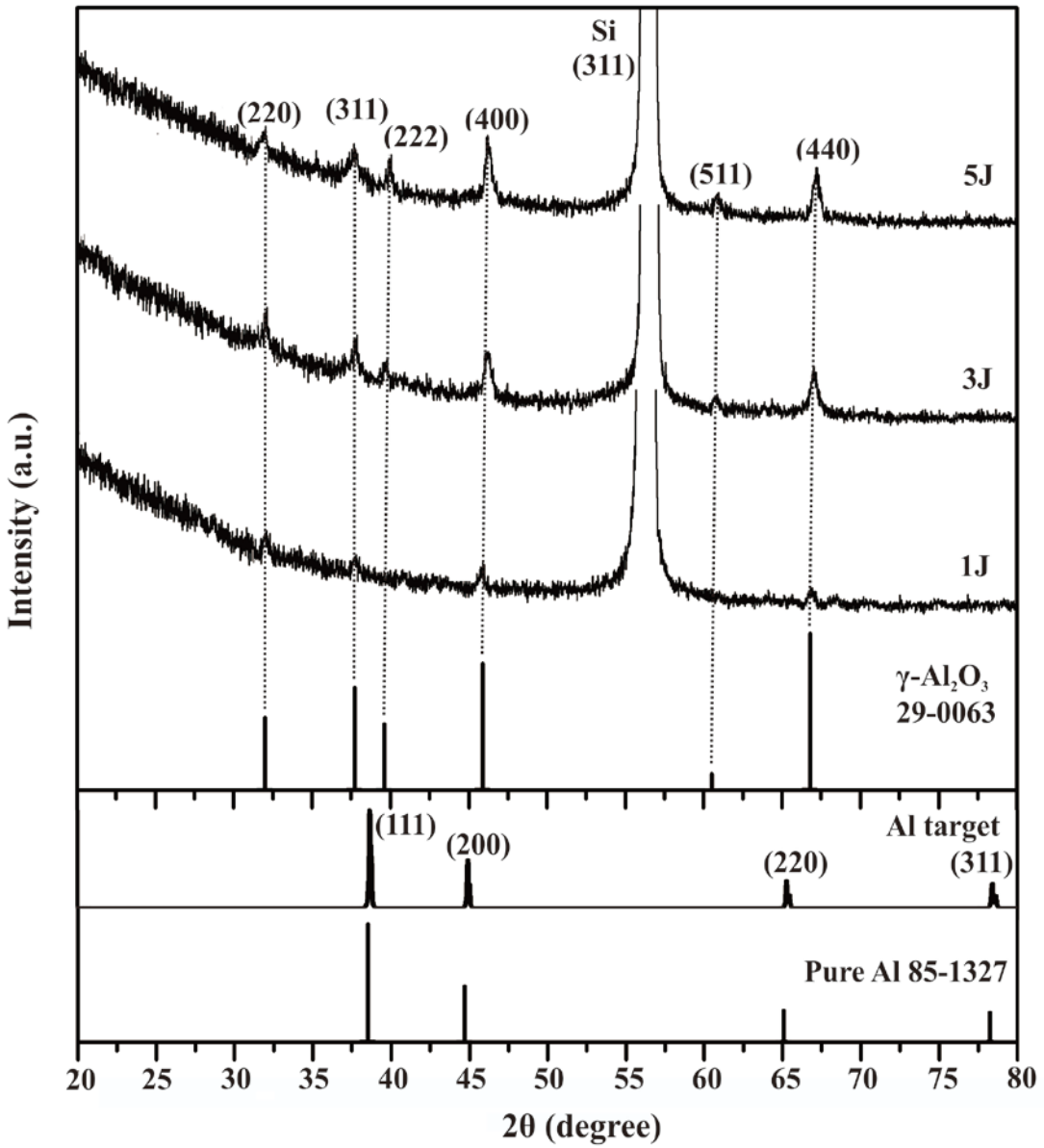

Figure 4.34 XRD patterns of pure Al and Al2O3 nanoparticles synthesized from laser energies of 1, 3, and 5 J.

4.7.6 Chemical structure (XPS)

In figure 4.35 are typical XPS survey scans of an alumina layer after laser ablation at different energies 1, 3 and 5 J for 5,000 pulses. To correct for sample charging, the spectra were shifted to set the C-C components of the C 1s core level peak at a binding energy of 284.8 eV. The results of spectra exhibit photoelectron peaks for the following transitions: O1s, O2s, C1s, N1s, Al 2s and Al 2p. The surface spectrum is indicative of an alumina surface contaminated by adventitious carbon and nitrogen in air

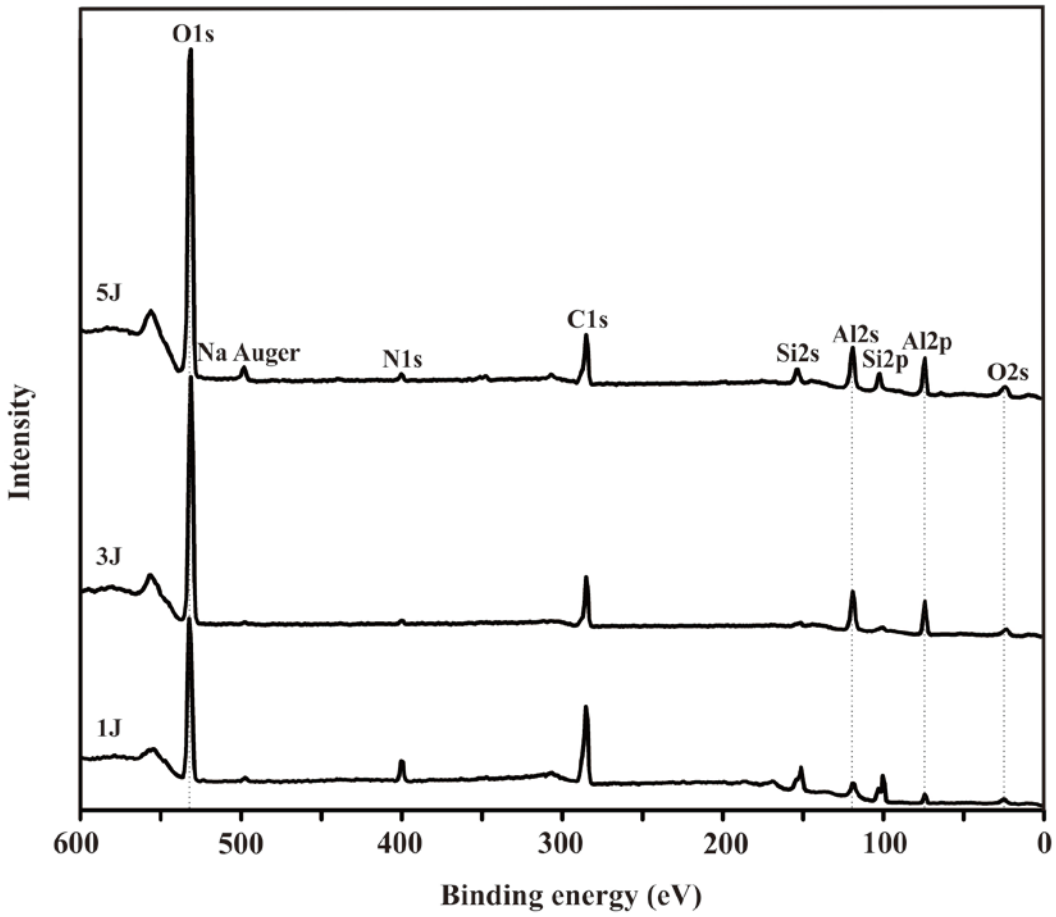

Figure 4.35 XPS survey scans of different laser energies 1, 3 and 5 J

The alumina nanoparticles were analyzed with X-ray photoelectron spectroscopy (XPS) and the analysis of Al2p 75.4 eV and O1s 532 eV XPS lines is reported in Figure.4.36-4.37. The spectra analysis has provided the composition of our nanoparticles giving an Al ratio of 0.307 and O ratio of 0.693 as shown in table 4.12, in good agreement with the stoichiometry of Al_2O_3[59]. Another satellite O1s structure has been found at a binding energy of 533.8 eV and ascribed to a differently bonded oxygen (adsorbed water). No complexity was found in the case of Al2p line.

Table 4.12 XPS results of chemical compositions at 300 V

Laser energy (J/Pulse)	Element	Atomic percentage %
1	Al	14.23
	O	85.77
3	Al	30.72
	O	69.28
5	Al	26.81
	O	73.19

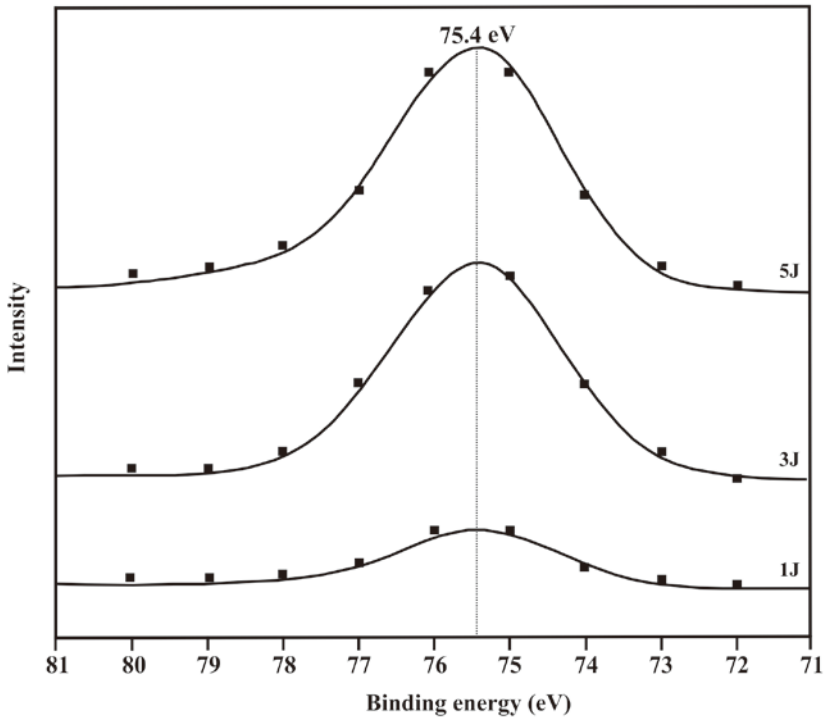

Figure 4.36 The analysis of Al2p at different energies 1, 3 and 5 J

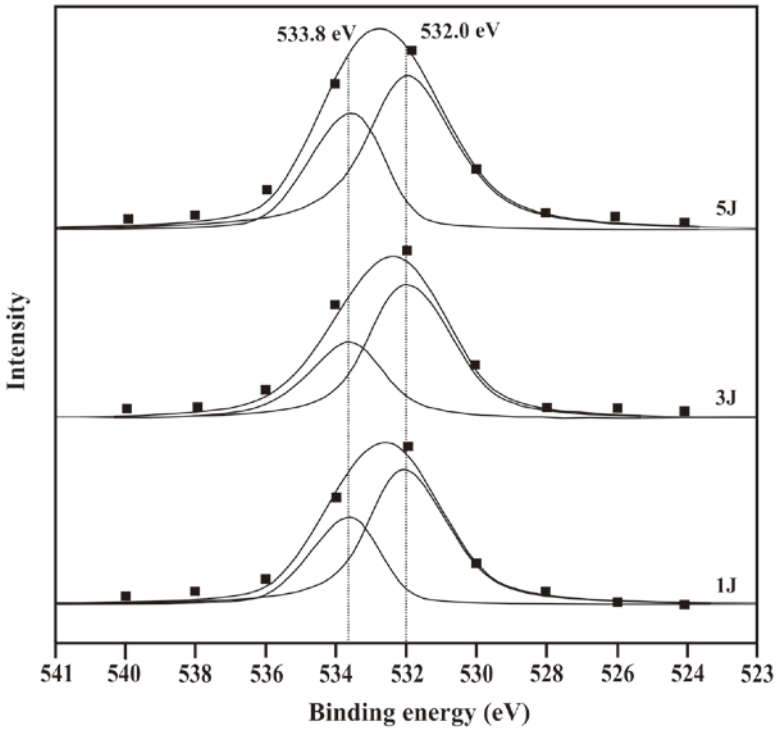

Figure 4.37 The analysis of O1s at different energies 1, 3 and 5 J